that connect them. The solution from a direct method can be used to identify such structure, and the approach considered in this Note can be adapted to handle it.

A motivating reason for using the Riccati dichotomic basis method is to gain insight into the phase space structure in the neighborhood of the optimal solution. Previously, an approximate dichotomic basis method was developed to solve completely hypersensitive HBVPs[2] and has been shown to work successfully on problems of moderate complexity.[3] The major disadvantage of the approximate dichotomic basis method is that it does not produce direct information about the exact directions of expanding and contracting behavior in the tangent space of the optimal trajectory. This deficiency is overcome by the Riccati dichotomic basis method described here. Not only does the Riccati dichotomic basis method produce a solution to the HBVP, but it also produces the solution to the Riccati differential equations from which the dichotomic basis can be constructed with no further computation. The dichotomic basis provides useful information about the conditions satisfied by points on the stable and unstable manifolds.

Finally, it is important to distinguish the successive approximation procedures developed here from the well-known backward sweep method presented in Ref. 9, which also solves a Riccati differential equation. The basic difference between the two methods is that the method of Ref. 9 makes no attempt to eliminate the hypersensitivity, whereas the key feature of the current method is that the hypersensitivity is eliminated over the time interval of interest. Consequently, for problems with relatively long durations in the boundary layers the method of Ref. 9 will be less likely to succeed than will the method developed in this Note.

Conclusions

A Riccati dichotomic basis has been constructed in the initial boundary-layer segments along the solution of completely hypersensitive HBVPs arising in optimal control. The structure of this basis has led to the development of a successive approximation procedure to find the solution in the initial boundary layer. The successive approximation procedure was illustrated on a problem in supersonic aircraft flight, and its range of applicability was briefly discussed.

Acknowledgments

This research was sponsored by the National Science Foundation and the California Space Institute. The author would like to thank Kenneth D. Mease of the University of California, Irvine, for his supervision as doctoral thesis advisor during the course of this research. The author would also like to thank S.-H. Lam of Princeton University, New Jersey, who provided valuable insight during the course of this research.

References

[1]Rao, A. V., and Mease, K. D., "Dichotomic Basis Approach to Solving Hyper-Sensitive Optimal Control Problems," *Automatica*, Vol. 35, No. 4, 1999, pp. 633–642.

[2]Rao, A. V., and Mease, K. D., "Eigenvector Approximate Dichotomic Basis Method for Solving Hyper-Sensitive Optimal Control Problems," *Optimal Control Applications and Methods*, Vol. 21, No. 1, 2000, pp. 1–19.

[3]Rao, A. V., "Application of a Dichotomic Basis Method to Performance Optimization of Supersonic Aircraft," *Journal of Guidance, Control, and Dynamics*, Vol. 23, No. 3, 2000, pp. 570–573.

[4]Lam, S. H., "Using CSP to Understand Complex Chemical Kinetics," *Combustion, Science, and Technology*, Vol. 89, No. 5–6, 1993, pp. 375–404.

[5]Lam, S. H., and Goussis, D. A., "The CSP Method for Simplifying Kinetics," *International Journal of Chemical Kinetics*, Vol. 26, 1994, pp. 461–486.

[6]Guckenheimer, J., and Holmes, P., *Nonlinear Oscillations, Dynamical Systems, and Bifurcations of Vector Fields*, Springer-Verlag, New York, 1990, pp. 12–16.

[7]Seywald, H., and Cliff, E. M., "Range Optimal Trajectories for an Aircraft Flying in the Vertical Plane," *Journal of Guidance, Control, and Dynamics*, Vol. 17, No. 2, 1994, pp. 389–398.

[8]Ardema, M. D., "Solution of the Minimum Time-to-Climb Problem by Matched Asymptotic Expansions," *AIAA Journal*, Vol. 14, No. 7, 1976, pp. 843–850.

[9]Bryson, A. E., and Ho, Y.-C., *Applied Optimal Control*, Hemisphere, New York, 1975, pp. 217, 218.

Stability and Convergence of a Hybrid Adaptive Feedforward Observer

Chau M. Tran*
North Carolina State University, Raleigh, North Carolina 27695
and
S. C. Southward†
Lord Corporation, Cary, North Carolina 27511

Introduction

In the active noise and vibration control field, as well as the field of flexible structures, it is common to require an estimation technique for predicting the appropriate system response where it is either physically impossible or undesirable to place an actual error sensor.[1–4] To resolve this virtual sensing estimation problem, especially for systems subjected to nonstationary tonal disturbances, Tran and Southward[5] proposed using a hybrid adaptive feedforward observer. This technique is a dynamic closed-loop transformation that estimates the system states using the sensor responses and a dynamic system model. Similar to other observer designs, the separation principle between the controller and the hybrid observer is confirmed.

The hybrid adaptive feedforward observer consists of two components. A conventional feedback component is used to stabilize the closed-loop observer, as well as to speed up the convergence process. In addition, it provides extra design freedom to minimize the effects of process and sensor noise. An adaptive feedforward component is used to track the unknown mapping of the nonstationary tonal disturbance onto the observer states. The adaptation was achieved using a least-mean-squares(LMS)-based gradient descent method.

In this Note, the stability and convergence of the hybrid observer is analyzed for the first time. It was proven that, in this design, the nonautonomous overall system dynamics indeed contains linear-time-invariant (LTI) eigenvalues. The analytical result on stability was demonstrated using a one-dimensional acoustic duct.

Problem Formulation

Consider a plant or dynamic system with a vector of outputs $\boldsymbol{y}$ obtained as the measured response from sensors, as shown in Fig. 1. A vector of unknown external disturbances $\boldsymbol{w}$ excites the plant as well as a vector of control inputs $\boldsymbol{u}$. No a priori knowledge of how the disturbance $\boldsymbol{w}$ actually affects the internal states of the plant is assumed; however, a feedforward reference signal, which is correlated to the disturbance in $\boldsymbol{w}$, is assumed to be available as indicated by the dotted line in the left half of Fig. 1.

The plant is represented in state-space notation with the mapping of the unknown external disturbance explicitly shown in the state equation as

$$\dot{\boldsymbol{x}} = \boldsymbol{A}\boldsymbol{x} + \boldsymbol{B}\boldsymbol{u} + \boldsymbol{w}, \qquad \boldsymbol{y} = \boldsymbol{C}\boldsymbol{x} + \boldsymbol{D}\boldsymbol{u} \tag{1}$$

Provided that the state-space model ($\boldsymbol{A}$, $\boldsymbol{C}$) is completely observable,[6] we first design a conventional observer to estimate the system states, assuming no disturbance input, that is, $\boldsymbol{w} = \boldsymbol{0}$. The conventional observer is then augmented with an adaptive feedforward

Received 9 December 2000; revision received 19 September 2001; accepted for publication 2 October 2002.

*Director of Educational Laboratories, Department of Mechanical and Aerospace Engineering.
†Staff Engineer, Thomas Lord Research Center.

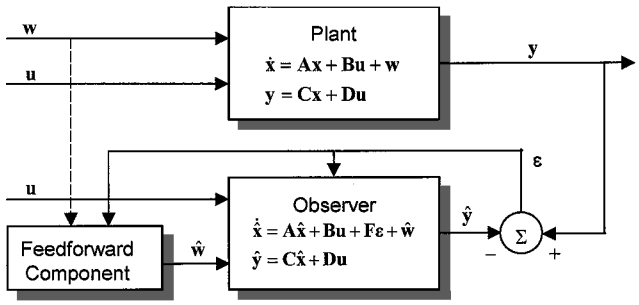

Fig. 1 Implementation of a hybrid adaptive feedforward observer.

component. The equations describing the hybrid observer are written as

$$\dot{\hat{\boldsymbol{x}}} = \boldsymbol{A}\hat{\boldsymbol{x}} + \boldsymbol{B}\boldsymbol{u} + \boldsymbol{F}\boldsymbol{\varepsilon} + \hat{\boldsymbol{w}}, \qquad \hat{\boldsymbol{y}} = \boldsymbol{C}\hat{\boldsymbol{x}} + \boldsymbol{D}\boldsymbol{u} \tag{2}$$

where $\boldsymbol{\varepsilon} \equiv \boldsymbol{y} - \hat{\boldsymbol{y}}$ is the output error vector.

In the special case where the disturbance frequency is known a priori and remains constant, a variety of fixed-gain feedback control strategies, based on the internal model principle, are available for rejecting the disturbance.[7–9] These techniques are not robust when the disturbance frequency is nonstationary and unknown.

Define the state reconstruction error to be $\boldsymbol{\rho} \equiv \boldsymbol{x} - \hat{\boldsymbol{x}}$; an equivalent error dynamic system is formed as

$$\dot{\boldsymbol{\rho}} = [\boldsymbol{A} - \boldsymbol{FC}]\boldsymbol{\rho} + (\boldsymbol{w} - \hat{\boldsymbol{w}}), \qquad \boldsymbol{\varepsilon}_p = \boldsymbol{C}\boldsymbol{\rho} \tag{3}$$

Equation (3) indicates that the feedback-gain matrix $\boldsymbol{F}$ is used to partially specify the convergence of the error dynamic system by appropriate pole placement. This feedback element can also provide some compensation for modeling errors and help reduce the sensitivity to sensor and/or process noise.[10] The feedforward component, on the other hand, rejects the nonstationary tonal disturbance present in the state reconstruction error.

For a single nonstationary tonal disturbance, without loss of generality, $\boldsymbol{w}$ can be expanded into in-phase and quadrature components as $\boldsymbol{w}(t) = \boldsymbol{g}_c \cos(\omega t) + \boldsymbol{g}_s \sin(\omega t)$, where $\boldsymbol{g}_c$ and $\boldsymbol{g}_s$ are unknown vectors that are potentially slowly time varying. The feedforward component $\hat{\boldsymbol{w}}$ in Eq. (2) is similarly defined as $\hat{\boldsymbol{w}}(t) = \hat{\boldsymbol{g}}_c(t)\cos(\omega t) + \hat{\boldsymbol{g}}_s(t)\sin(\omega t)$. From this formulation, it is clear that, if $\hat{\boldsymbol{g}}_c$ approaches $\boldsymbol{g}_c$, and $\hat{\boldsymbol{g}}_s$ approaches $\boldsymbol{g}_s$, then the state reconstruction error can be reduced to zero. An LMS-based adaptive algorithm can be designed to achieve this objective.

The adaptive coefficients $\hat{\boldsymbol{g}}_c$ and $\hat{\boldsymbol{g}}_s$ are to be updated in a direction that minimizes the cost function $J = \frac{1}{2}\boldsymbol{\varepsilon}^T(t)\boldsymbol{\varepsilon}(t)$. Let $\boldsymbol{H}_R(\omega)$ and $\boldsymbol{H}_I(\omega)$ be the real and imaginary parts of the closed-loop observer transfer function, $\boldsymbol{H}(j\omega) \equiv \boldsymbol{C}[j\omega\boldsymbol{I} - (\boldsymbol{A} - \boldsymbol{FC})]^{-1}$, the final LMS-based adaptation laws for the feedforward disturbance estimates become[5]

$$\dot{\hat{\boldsymbol{g}}}_c(t) = \mu\nabla_c(t)\boldsymbol{\varepsilon}(t), \qquad \dot{\hat{\boldsymbol{g}}}_s(t) = \mu\nabla_s(t)\boldsymbol{\varepsilon}(t) \tag{4}$$

where $\nabla_c(t) \equiv [\boldsymbol{H}_R^T(\omega)\cos(\omega t) - \boldsymbol{H}_I^T(\omega)\sin(\omega t)]$ and $\nabla_s(t) \equiv [\boldsymbol{H}_I^T(\omega)\cos(\omega t) + \boldsymbol{H}_R^T(\omega)\sin(\omega t)]$. This simplification takes explicit advantage of the orthogonal reference signals, which are assumed to be available; μ is the adaptive step size that governs the convergence rate. As the disturbance frequency varies, a new corresponding set of matrices $\boldsymbol{H}_R(\omega)$ and $\boldsymbol{H}_I(\omega)$ are required for proper evaluation of the gradient terms in Eq. (4). For linear systems, this observer may be extended to handle disturbances that contain multiple tones. The implementation of the feedforward component is shown in Fig. 2.

Stability and Convergence

Consider the overall system dynamics

$$\dot{z} = \mathcal{M}(t)z + Qr \tag{5}$$

where $z = [\boldsymbol{x}^T \;\; \hat{\boldsymbol{x}}^T \;\; \hat{\boldsymbol{g}}_c^T \;\; \hat{\boldsymbol{g}}_s^T]^T$, $r = [\boldsymbol{u}^T \;\; \boldsymbol{w}^T]^T$, and

$$Q = \begin{bmatrix} \boldsymbol{B}^T & \boldsymbol{B}^T & \boldsymbol{0} & \boldsymbol{0} \\ \boldsymbol{I} & \boldsymbol{0} & \boldsymbol{0} & \boldsymbol{0} \end{bmatrix}^T$$

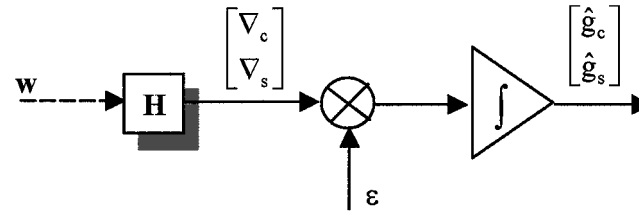

Fig. 2 Implementation of the adaptive feedforward component.

In the presence of the adaptive feedforward components $\hat{\boldsymbol{g}}_c$ and $\hat{\boldsymbol{g}}_s$, system (5) becomes a nonautonomous system. In other words, the mathematical model of the system is now time varying. The elements of the state matrix are explicitly time dependent in the sine and cosine terms. In general, very few nonautonomous systems have rigorous stability proofs.

The state matrix for the overall system dynamics can be partitioned as

$$\mathcal{M}(t) = \begin{bmatrix} \boldsymbol{A} & \boldsymbol{0} & \boldsymbol{0} & \boldsymbol{0} \\ \boldsymbol{FC} & \boldsymbol{A} - \boldsymbol{FC} & \cos(\omega t)\boldsymbol{I} & \sin(\omega t)\boldsymbol{I} \\ \mu\nabla_c\boldsymbol{C} & -\mu\nabla_c\boldsymbol{C} & \boldsymbol{0} & \boldsymbol{0} \\ \mu\nabla_s\boldsymbol{C} & -\mu\nabla_s\boldsymbol{C} & \boldsymbol{0} & \boldsymbol{0} \end{bmatrix} = \begin{bmatrix} \boldsymbol{A} & \boldsymbol{0}_{n\times 3n} \\ \mathcal{M}_1(t) & \mathcal{M}_2(t) \end{bmatrix} \tag{6}$$

$\boldsymbol{I}$ is the identity matrix of an appropriate order. In this case, the order is the number of states or n. $\mathcal{M}(t)$ is a $4n \times 4n$ matrix. Equation (6) shows that $\boldsymbol{F}$ and μ must be selected to maintain system stability. Furthermore, matrix $\mathcal{M}(t)$ contains different combinations of "slow" and "fast" eigenvalues with different associated $\boldsymbol{F}$ and μ. Therefore, the optimal $\boldsymbol{F}$ and μ will be those that construct a combination of eigenvalues such that the error dynamic system can converge the fastest.

Stability is analyzed from the determinant of the matrix $[\lambda\boldsymbol{I} - \mathcal{M}(t)]$. Because $[\lambda\boldsymbol{I} - \mathcal{M}(t)]$ is a lower triangular block matrix with square diagonal blocks, its determinant is calculated as[11]

$$|\lambda\boldsymbol{I} - \mathcal{M}(t)| = |\lambda\boldsymbol{I} - \boldsymbol{A}||\lambda\boldsymbol{I} - \mathcal{M}_2(t)| \tag{7}$$

Equation (7) shows the separation principle. The first term in the right-hand side of Eq. (7) provides the eigenvalues of the open-loop system. These poles are time invariant.

Now consider the second term in Eq. (7). For notational convenience, $\boldsymbol{s}$ and $\boldsymbol{c}$ will be used as abbreviations for $\sin(\omega t)$ and $\cos(\omega t)$. A column reduction is performed on the last two block columns as

$$\begin{aligned} |\lambda\boldsymbol{I} - \mathcal{M}_2(t)| &= \begin{vmatrix} \lambda\boldsymbol{I} - (\boldsymbol{A} - \boldsymbol{FC}) & -\boldsymbol{cI} & -\boldsymbol{sI} \\ \mu\nabla_c\boldsymbol{C} & \lambda\boldsymbol{I} & \boldsymbol{0} \\ \mu\nabla_s\boldsymbol{C} & \boldsymbol{0} & \lambda\boldsymbol{I} \end{vmatrix} \\ &= \frac{1}{-\boldsymbol{c}^n\boldsymbol{s}^n}\begin{vmatrix} \cdots & -\boldsymbol{csI} & \boldsymbol{csI} \\ \cdots & \lambda\boldsymbol{sI} & \boldsymbol{0} \\ \cdots & \boldsymbol{0} & -\lambda\boldsymbol{cI} \end{vmatrix} \\ &= \frac{1}{-\boldsymbol{c}^n}\begin{vmatrix} \cdots & -\boldsymbol{cI} & \boldsymbol{0} \\ \cdots & \lambda\boldsymbol{I} & \lambda\boldsymbol{sI} \\ \cdots & \boldsymbol{0} & -\lambda\boldsymbol{cI} \end{vmatrix} \end{aligned} \tag{8}$$

A row reduction is now performed on the last two block rows of the subsequent matrix:

$$\begin{aligned} |\lambda\boldsymbol{I} - \mathcal{M}_2(t)| &= \frac{1}{-\boldsymbol{c}^{2n}\boldsymbol{s}^n}\begin{vmatrix} \lambda\boldsymbol{I} - (\boldsymbol{A} - \boldsymbol{FC}) & -\boldsymbol{cI} & \boldsymbol{0} \\ \mu\boldsymbol{c}\nabla_c\boldsymbol{C} & \lambda\boldsymbol{cI} & \lambda\boldsymbol{csI} \\ \mu\boldsymbol{s}\nabla_s\boldsymbol{C} & \boldsymbol{0} & -\lambda\boldsymbol{csI} \end{vmatrix} \\ &= \frac{1}{-\boldsymbol{c}^{2n}}\begin{vmatrix} \lambda\boldsymbol{I} - (\boldsymbol{A} - \boldsymbol{FC}) & -\boldsymbol{cI} & \boldsymbol{0} \\ \mu[\boldsymbol{c}\nabla_c + \boldsymbol{s}\nabla_s]\boldsymbol{C} & \lambda\boldsymbol{cI} & \boldsymbol{0} \\ \mu\nabla_s\boldsymbol{C} & \boldsymbol{0} & -\lambda\boldsymbol{cI} \end{vmatrix} \end{aligned} \tag{9}$$

The lower triangular matrix with square diagonal blocks in Eq. (9) is further expanded as

$$|\lambda \boldsymbol{I} - \mathcal{M}_2(t)| = \frac{1}{-\boldsymbol{c}^{2n}} \begin{vmatrix} \lambda \boldsymbol{I} - (\boldsymbol{A} - \boldsymbol{FC}) & -\boldsymbol{cI} \\ \mu[\boldsymbol{c}\nabla_c + \boldsymbol{s}\nabla_s]\boldsymbol{C} & \lambda \boldsymbol{cI} \end{vmatrix} |-\lambda \boldsymbol{cI}|$$

$$= \begin{vmatrix} \lambda \boldsymbol{I} - (\boldsymbol{A} - \boldsymbol{FC}) & -\boldsymbol{I} \\ \mu[\boldsymbol{c}\nabla_c + \boldsymbol{s}\nabla_s]\boldsymbol{C} & \lambda \boldsymbol{I} \end{vmatrix} |\lambda \boldsymbol{I}| \tag{10}$$

Substituting ∇_c and ∇_s into Eq. (10) gives

$$|\lambda \boldsymbol{I} - \mathcal{M}_2(t)| = \begin{vmatrix} \lambda \boldsymbol{I} - (\boldsymbol{A} - \boldsymbol{FC}) & -\boldsymbol{I} \\ \mu \boldsymbol{H}_R^T(\omega)\boldsymbol{C} & \lambda \boldsymbol{I} \end{vmatrix} |\lambda \boldsymbol{I}| \tag{11}$$

Equation (11) shows two distinct sets of eigenvalues. One contains zero eigenvalues, and the other contains the eigenvalues of the hybrid observer. More important, these eigenvalues are those of an LTI system.

The analysis has proven that, although our system is nonautonomous due to the presence of the adaptive feedforward component, with the implementation of orthogonal reference signals in the LMS-based gradient descent method, the eigenvalues become those of an LTI system. Consequently, we can take full advantage of the existing classical techniques to examine its stability. Because it is practical to observe the system eigenvalues when determining stability limits, the root locus technique was chosen. For a given plant and a nonzero feedback matrix $\boldsymbol{F}$ for the observer, there exists an adaptive step size μ such that all eigenvalues remain in the left-half plane. The analytical result was demonstrated using a one-dimensional acoustic duct.

Demonstration

The test bed for demonstrating stability analysis was a one-dimensional acoustic duct with a rigid termination at one end, and a disturbance excitation speaker at the opposite end (Fig. 3). This system is a standard linear distributed parameter system in acoustics. The physical dimensions of the acoustic duct were selected based on a 300-Hz signal conditioning bandwidth limit and channel limitations of the real-time hardware used for this implementation of the algorithm. A duct length of $L = 2.88$ m and a diameter of $D = 0.15$ m were chosen. With these dimensions, the longitudinal resonance frequencies are multiples of 60 Hz. The first five modes lie within the 300-Hz bandwidth limitation, and the first radial mode only begins to participate well above this limit.

To form a linear array, 12 equally spaced microphones were placed along the interior duct wall. The pressure measurements at a selection of these microphones are the outputs of the state-space system (1). First, the frequency responses between the excitation source and all 12 microphones were measured and input to the SmartID toolbox[12] to generate an 11th-order continuous-time empirical state-space model. The $\boldsymbol{B}$ and $\boldsymbol{D}$ matrices from this empirical model were discarded because only the $\boldsymbol{A}$ and $\boldsymbol{C}$ matrices were required. In a practical application, the $\boldsymbol{A}$, $\boldsymbol{B}$, $\boldsymbol{C}$, and $\boldsymbol{D}$ matrices associated with the secondary sources would be used. Next, a set of microphones was chosen such that $\boldsymbol{A}$ and $\boldsymbol{C}$ are completely observable. Among the possibilities, the microphones 3, 5, and 11 were chosen; thus, a plant with appropriate states and outputs according to Eq. (1) was established to demonstrate stability.

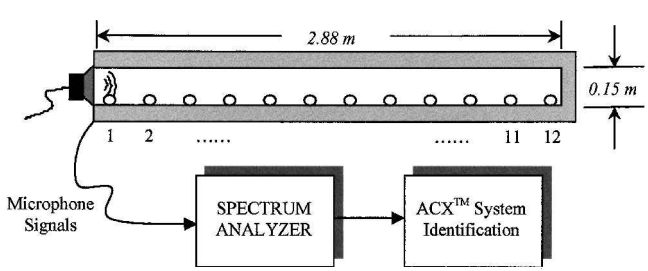

Fig. 3 Construction of the empirical state space model for the one-dimensional acoustic duct.

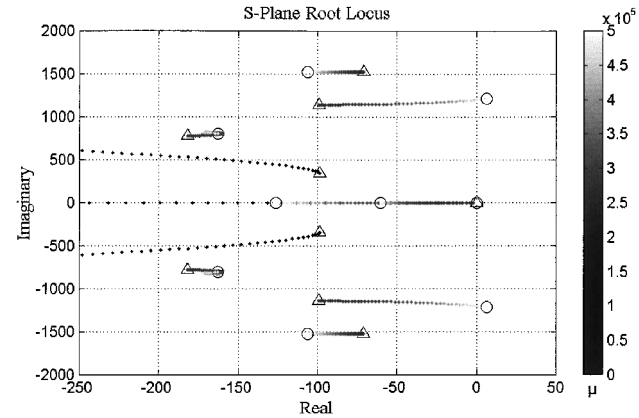

Fig. 4 Demonstration of the use of root locus technique on an acoustic duct and its observer at the first resonance (60 Hz).

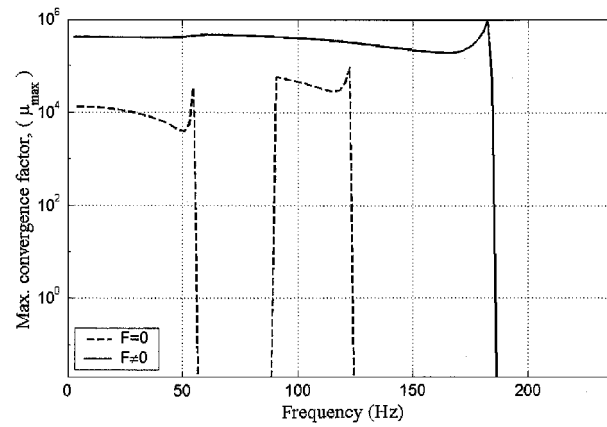

Fig. 5 Upper limit of the adaptive step size for the hybrid observer used in an acoustic duct system.

The system stability was first demonstrated at the fundamental resonance. The feedback gain matrix $\boldsymbol{F}$ was selected to move all poles of the equivalent error dynamic system (3) four times farther into the left-half plane than the nominal plant poles. The adaptive convergence factor μ was then increased until the poles crossed into the right-half plane. Figure 4 shows the root locus of the overall system dynamics (5) when the acoustic duct was excited at 60 Hz. In Fig. 4, poles at $\mu = 0$ are represented by triangles. Poles at the upper bound of μ are represented by circles. For the acoustic duct system, the pole corresponding to the third mode is the first to become unstable as μ approaches 4.5×10^5.

Suppose it is now desirable to demonstrate the system stability over a range of frequency. $\boldsymbol{F}$ again was chosen such that all poles of the equivalent error dynamic system are four times farther into the left-half plane than the nominal plant poles. From 0 to 200 Hz, a series of root loci similar to Fig. 4 was generated. The upper limit of the adaptive step size as a function of frequency was then summarized (Fig. 5). It can be seen that, at any frequency, there indeed exists an upper limit for the adaptive step size μ such that the system remains stable. As expected from the root locus of Fig. 4, the maximum adaptive step size at 60 Hz is approximately 4.5×10^5.

The same approach was additionally used to examine the stability for a special case when the feedback component of the observer was neglected. Figure 5 shows the necessity of the feedback component in the regions of 60–90 Hz and 125–180 Hz. For the chosen acoustic system, the feedback matrix $\boldsymbol{F}$ not only supplements the adaptive control in these regions, but also raises the stability limit for the entire domain, which ultimately increases the convergence rate.

Conclusions

We investigated the stability and convergence of a hybrid observer, which contains a conventional closed-loop observer as well as an adaptive feedforward component, for systems subjected to nonstationary tonal disturbances. This design follows the separation

principle like any other observers. The primary purpose of the feedback component is to partially specify the convergence of the equivalent error dynamic system and to provide additional freedom to minimize the effects of process and sensor noise. The adaptive feedforward component was designed to estimate the presumed effect of the tonal disturbance on the actual plant states, using an LMS-based gradient descent method. Because of the presence of the feedforward component, the overall system dynamics becomes nonautonomous. This nonautonomous system, however, was proven to contain LTI eigenvalues when orthogonal reference signals were implemented. Consequently, classical techniques could be used to study its stability. The analytical results were demonstrated by applying the root locus technique to a one-dimensional acoustic duct. It was confirmed that, for a plant with a particular feedback gain for the observer, there exists an adaptive step size such that the system is stable.

References

[1]Kammer, D. C., "Estimation of Structural Response Using Remote Sensor Locations," *Journal of Guidance, Control, and Dynamics*, Vol. 20, No. 3, 1997, pp. 501–508.

[2]Popovich, S. R., "Active Acoustic Control in Remote Regions," U.S. Patent 5,701,350, filed Dec. 1997.

[3]Garcia-Bonito, J., Elliott, S. J., and Boucher, C. C., "A Virtual Microphone Arrangement in a Practical Active Headrest," *Proceedings of Internoise 96*, Inst. of Acoustics, St. Albans, UK, pp. 1115–1120.

[4]Elliott, S. J., "Active Sound Control Systems and Sound Reproduction Systems," U.S. Patent 5,381,485, filed Jan. 1995.

[5]Tran, C. M., and Southward, S. C., "A Virtual Sensing Method for Tonal ANVC Systems," *Journal of Dynamic Systems, Measurement, and Control*, Vol. 124, No. 1, 2002, pp. 35–40.

[6]Brogan, W. L., *Modern Control Theory*, 3rd ed., Prentice–Hall, Upper Saddle River, NJ, 1991, pp. 461–474.

[7]Messner, W., and Bodson, M., "Design of Adaptive Feedforward Algorithms Using Internal Model Equivalence," *International Journal of Adaptive Control and Signal Processing*, Vol. 9, March–April 1995, pp. 199–212.

[8]Franklin, G. F., Powell, J. D., and Emami-Naeini, A., *Feedback Control of Dynamic Systems*, 3rd ed., Addison–Wesley, Reading, MA, 1994, pp. 560–564.

[9]Davison, E. J., "The Robust Control of a Servomechanism Problem for Linear Time-Invariant Multivariable Systems," *IEEE Transactions on Automatic Control*, Vol. AC-21, No. 1, 1976, pp. 25–34.

[10]Kwakernaak, H., and Sivan, R., *Linear Optimal Control Systems*, Wiley-Interscience, New York, 1972, pp. 339–361.

[11]Kailath, T., *Linear Systems*, Prentice–Hall, Englewood Cliffs, NJ, 1980, pp. 650, 651.

[12]ACX™, SmartID System Identification Software, Version 1.0.1, Active Control Experts, Inc., Cambridge, MA, 1995.